Article

Sulfur-Doped Organosilica Nanodots as a Universal Sensor for Ultrafast Live/Dead Cell Discrimination

Yan-Hong Li †, Jia Zeng †, Zihao Wang, Tian-Yu Wang, Shun-Yu Wu, Xiao-Yu Zhu, Xinping Zhang, Bai-Hui Shan, Cheng-Zhe Gao, Shi-Hao Wang and Fu-Gen Wu *

State Key Laboratory of Bioelectronics, School of Biological Science and Medical Engineering, Southeast University, 2 Sipailou Road, Nanjing 210096, China
* Correspondence: wufg@seu.edu.cn
† These authors contributed equally to this work.

Abstract: Rapid and accurate differentiation between live and dead cells is highly desirable for the evaluation of cell viability. Here, we report the application of the orange-emitting sulfur-doped organosilica nanodots (S-OSiNDs) for ultrafast (30 s), ultrasensitive (1 µg/mL), and universal staining of the dead bacterial, fungal, and mammalian cells but not the live ones, which satisfies the requirements of a fluorescent probe that can specifically stain the dead cells. We further verify that the fluorescence distribution range of S-OSiNDs (which are distributed in cytoplasm and nucleus) is much larger than that of the commercial dead/fixed cell/tissue staining dye RedDot2 (which is distributed in the nucleus) in terms of dead mammalian cell staining, indicating that S-OSiNDs possess a better staining effect of dead cells than RedDot2. Overall, S-OSiNDs can be used as a robust fluorescent probe for ultrafast and accurate discrimination between dead and live cells at a single cell level, which may find a variety of applications in the biomedical field.

Keywords: nanoprobe; fluorescence imaging; live/dead staining; bacteria; mammalian cells; fungi

1. Introduction

Rapidly, sensitively, and accurately distinguishing between live and dead cells is of tremendous significance to various biomedical fields, such as cancer therapy and microbial infection treatment [1–7]. However, a simple and efficient method for fast and accurate live/dead cell discrimination at a single-cell level is still lacking, and additionally, some existing methods, such as atomic force microscopy [8], Fourier transform infrared spectroscopy [9], electron microscopy [10,11], Raman spectroscopy [12,13], and nucleic acid sequence-based amplification [14], are complicated, expensive, time-consuming, and laborious, seriously restricting their practical applications in the discrimination between live and dead cells.

In recent years, fluorescence labeling technology has gained much attention due to its outstanding advantages, including rapid response, simple operation, high sensitivity, ease of quantification, etc. [15–21]. The frequently used fluorescent reagents capable of realizing the discrimination between live and dead cells include SYTOX Green nucleic acid stain [22,23], propidium iodide (PI) [24], rhodamine 123 [25], fluorescein derivatives [26–28], calcein acetoxymethyl ester [29], RedDot2 [30], and carbon dots [31–38]. Most of these reagents selectively stain the dead cells via penetrating compromised cell membranes and staining the cell nucleus (e.g., RedDot2). However, these commercial dyes are relatively expensive, sometimes toxic, and require a long staining time before imaging. Carbon dots (a class of alternative materials for staining dead cells) usually have multicolor fluorescence emission, which overlaps with that of the live cell probes and severely limits their practical applications. Therefore, developing economical, low-toxic, and rapid imaging reagents with excellent optical properties for the discrimination between live and dead cells is highly required.

Fluorescent silicon nanoparticles (SiNPs), with satisfactory biocompatibility, outstanding photoluminescence stability, and convenient surface modification property [39], have been extensively applied in organic solar cells [40], antibacterial application [41,42], drug delivery [43], cancer therapy [44,45], sensing [46–51], and bioimaging [3,52–54]. Organosilica nanodots (OSiNDs) are one typical type of SiNPs prepared from organic silane molecules. In a previous research, our group fabricated OSiNDs through the hydrothermal treatment of rose bengal (RB) and 3-[2-(2-aminoethylamino)ethylamino]propyl-trimethoxysilane, and the OSiNDs possess the properties of small size (2.0 nm) and green fluorescence emission (525 nm) [54]. The OSiNDs were applied as an imaging reagent for lysosomal imaging for various types of cells and cells in different states (such as living, fixed, and permeabilized cells). Besides, in a later study, the OSiNDs were also applied for the wash-free, rapid, and universal staining of dead mammalian, bacterial, and fungal cells [3]. In addition, our group prepared another type of OSiNDs via a one-step hydrothermal reaction of an epoxy group-containing silane molecule, 3-glycidoxypropyltrimethoxysilane (GPTMS), and RB, and the resulting OSiNDs possessed the properties of small size (3.7 nm) and green fluorescence emission (529 nm) [42]. The OSiNDs were applied as an imaging reagent for visualizing various bacteria/biofilms. However, the above-mentioned OSiNDs all possess relatively short emission wavelengths (green fluorescence), which may decrease the imaging accuracy and limit further applications in organs or tissues in vivo. Besides, up till now, there is only one kind of OSiNDs that can be used for the fluorescence imaging-based discrimination between live and dead cells [3]. Therefore, the development of a sensitive and rapid fluorescent probe with long emission wavelengths (orange, red, or near-infrared fluorescence) for live/dead cell discrimination is highly desirable.

In 2021, we prepared orange-emitting sulfur-doped OSiNDs (S-OSiNDs) with a photoluminescence quantum yield (PLQY) of 13.4% (solvent: water) by the solvothermal treatment of citric acid, urea, and bis[3-(triethoxysilyl)propyl]tetrasulfide in *N*, *N*-dimethylformamide (DMF) at 200 °C for 12 h [51]. The S-OSiNDs realized the detection of multiple metal ions and achieved cancer/normal cell discrimination. Besides, the metal ion-induced fluorescence quenching of S-OSiNDs could be selectively restored by glutathione (GSH), and thus the metal ion-treated S-OSiNDs exhibited a sensitive GSH detection capability. Here, we demonstrate that the same S-OSiNDs can be used as a fluorescent probe for the differentiation between live and dead microbial (bacterial and fungal) and mammalian cells (Scheme 1). The S-OSiNDs can realize ultrafast (30 s), highly sensitive (required dose of S-OSiNDs: 1 μg/mL), accurate, universal, and selective staining of dead cells. Compared with RedDot2 (a commercial far-red cell membrane-impermeant nuclear dye suitable for selective dead/fixed cell/tissue staining), the fluorescence distribution range of S-OSiNDs (which are distributed in cytoplasm and nucleus) is much larger than that of RedDot2 (which is distributed in the nucleus) in terms of dead mammalian cell staining. The results indicate that S-OSiNDs possess a better staining effect of dead cells than RedDot2 and represent a promising probe for accurate discrimination between live and dead cells.
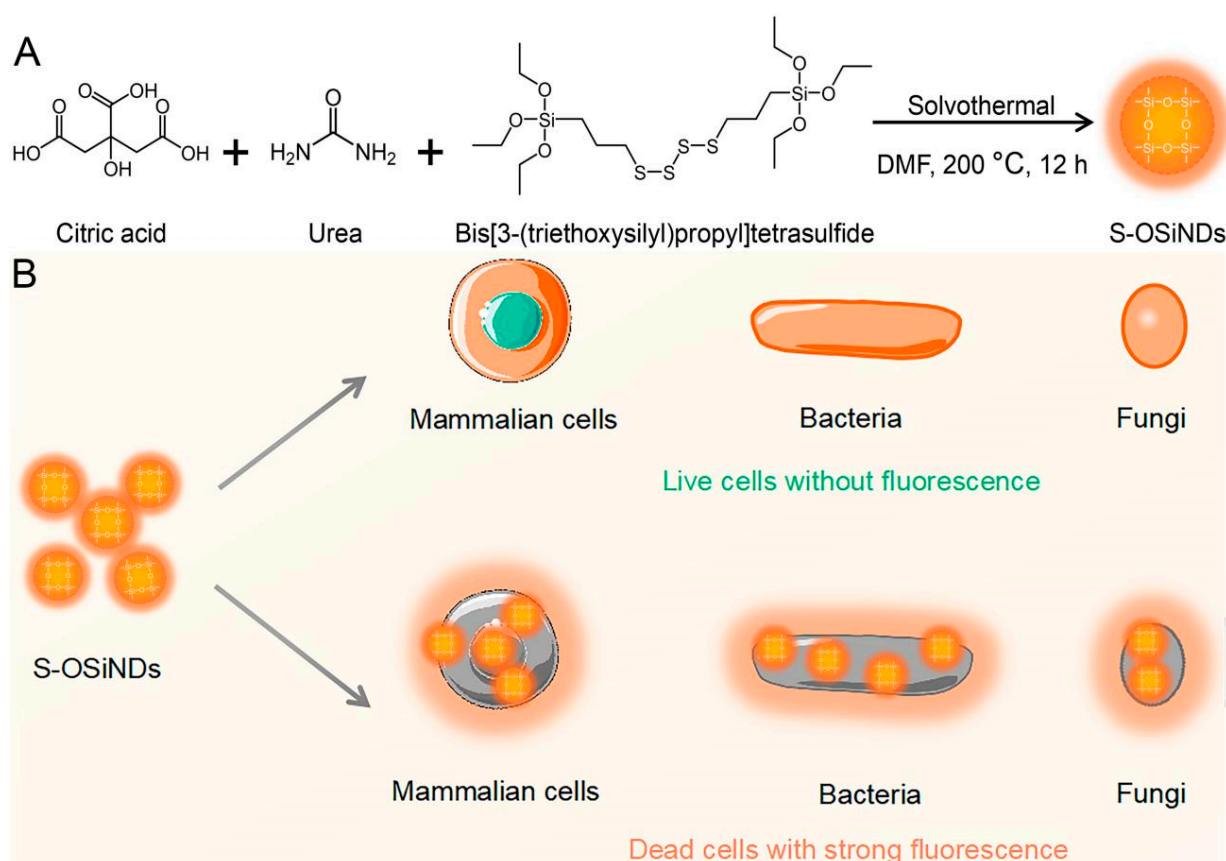
Scheme 1. Scheme depicting (**A**) the synthesis of S-OSiNDs and (**B**) their application for the discrimination between live and dead cells.

2. Materials and Methods

2.1. Preparation of Live/Dead Cells

For bacterial (*Escherichia coli* (*E. coli*) and *Staphylococcus aureus* (*S. aureus*)) and fungal cells (*Saccharomyces cerevisiae* (*S. cerevisiae*) yeast), the cells (10^8 colonies forming unit (CFU)/mL) were centrifugated (8000 rpm, 5 min) and then collected after being washed with physiological saline. Then, the cells were divided into two groups (live and dead groups). The cells in the dead group were treated with 1% benzalkonium bromide solution for 2 h, followed by washing with physiological saline. The cells in the live group were resuspended in physiological saline. For mammalian cells (HPAEpiCs (normal human pulmonary alveolar epithelial cells) and A549 (human lung cancer cells)), the cells were cultured in a 96-well glass bottom plate (5×10^3 cells/well). Next, the dead cells were obtained after treating the cells with ethanol for 10 min, while the live cells were incubated in Dulbecco's modified Eagle's medium (DMEM).

2.2. Evaluation of the Staining Performance of S-OSiNDs toward Live and Dead Bacteria

Live/dead *E. coli* and *S. aureus* cells (10^8 CFU/mL) were separately treated with different concentrations of S-OSiNDs (0, 1, 2, 5, 10, 20, and 50 µg/mL) for different time periods (30 s, 1, 2, 5, 10, and 30 min). Then, the cells were washed with physiological saline for 3 times and evaluated by flow cytometry using a flow cytometer (NovoCyte 2070R, ACEA Biosciences Inc., San Diego, CA, USA). In addition, the treated cells were imaged under a confocal microscope (TCS SP8, Leica, Wetzlar, Germany) at an excitation wavelength of 552 nm.

2.3. Evaluation of the Staining Performance of S-OSiNDs toward Live and Dead Fungi

For confocal imaging, the live/dead *S. cerevisiae* cells (10^8 CFU/mL) were exposed to different concentrations of S-OSiNDs (1, 2, 5, 10, 20, and 50 μg/mL) for different time periods (30 s, 1, 2, 5, 10, and 30 min), and then imaged using the confocal microscope at an excitation wavelength of 552 nm. For flow cytometry analysis, the live/dead *S. cerevisiae* cells (10^8 CFU/mL) were first exposed to different concentrations of S-OSiNDs (0, 1, 2, 5, 10, 20, and 50 μg/mL) for different time periods (30 s, 1, 2, 5, 10, and 30 min). Then, after washing the treated fungal cells with physiological saline for 3 times, we quantified the cellular fluorescence intensities by flow cytometry.

2.4. Evaluation of the Staining Performance of S-OSiNDs toward Normal and Cancerous Mammalian Cells

For confocal imaging, the normal/cancerous mammalian cells (HPAEpiC/A549) were mixed with different concentrations of S-OSiNDs (1, 2, 5, 10, 20, or 50 μg/mL) for different time periods (30 s, 1, 2, 5, 10, or 30 min). Afterward, the cells were imaged under the confocal microscope at an excitation wavelength of 552 nm. For flow cytometry analysis, the live/dead HPAEpiCs and A549 cells were first treated with different concentrations of S-OSiNDs (0, 1, 2, 5, 10, 20, or 50 μg/mL) for different time periods (30 s, 1, 2, 5, 10, or 30 min). Then, after washing the treated HPAEpiCs and A549 cells with phosphate-buffered saline (PBS, pH 7.4) for 3 times, we measured the cellular fluorescence intensities using flow cytometry.

2.5. Comparison between S-OSiNDs and RedDot2 on the Live/Dead Cell Discrimination Performance

To compare the live/dead differentiation performance of S-OSiNDs and RedDot2 (a commercial dye for nuclear DNA imaging), the live/dead bacteria (*E. coli/S. aureus*), fungi (*S. cerevisiae* yeast), and normal/cancerous mammalian cells (HPAEpiC/A549) were stained by the mixture of S-OSiNDs (5 μg/mL) and RedDot2 (diluted with physiological saline (for bacteria and fungi)/PBS (for mammalian cells) using a 1:200 ratio) for 10 min in the dark. Then the cells were imaged by the confocal microscope. The excitation wavelength of S-OSiNDs was 552 nm, while that of RedDot2 was 638 nm. Since the fluorescence emission color of S-OSiNDs was orange, which might be interfered with that of RedDot2 (red), the imaging color of S-OSiNDs was set as green.

3. Results and Discussion

3.1. Staining Performance of S-OSiNDs for Live and Dead Bacteria

S-OSiNDs were prepared according to our previous report [51]. The as-prepared S-OSiNDs exhibit a uniform size distribution with an average size of 1.3 ± 0.3 nm (Figure S1A,B, Supplementary Materials). The ultraviolet–visible (UV–vis) absorption spectrum of the S-OSiNDs shows an absorption peak at 335 nm and two broad absorption bands centering at around 470 and 558 nm, the latter of which is related to the fluorescence excitation of S-OSiNDs (Figure S1C). As shown by the fluorescence emission spectra, S-OSiNDs display excitation-independent fluorescence emission with the maximum excitation and emission peaks at 558 and 583 nm, respectively (Figure S1D,E). Besides, the PLQY of S-OSiNDs in water was calculated to be 13.4%. The Fourier transform infrared spectroscopy (FTIR) and X-ray photoelectron spectroscopy (XPS) data demonstrated that the obtained S-OSiNDs possess various groups/moieties, including C–H, O–H/N–H, C–O/C–N, C–C, Si–O, C=O, C–S, etc. (Figure S1F–I).

To evaluate if S-OSiNDs can be adapted to distinguish between live and dead bacterial cells, we chose *E. coli* and *S. aureus* as the representatives of the Gram-negative and Gram-positive bacteria, respectively. The results in Figures 1A and 2A revealed that the live bacterial cells (both *E. coli* and *S. aureus*) were hardly labeled by all the tested concentrations of S-OSiNDs, while the dead cells were observed to exhibit strong fluorescence signals. According to the flow cytometric results (Figures 1B–D and 2B–D), the

dead cells exhibited much higher fluorescence intensities than the live ones. Also, the effect of staining time on the live/dead cell discrimination performance of S-OSiNDs was further evaluated (Figures 3 and 4). Strong fluorescence signals were observed for the dead cells after incubation with S-OSiNDs after 30 s, whereas the live cells that we treated with S-OSiNDs for different time periods did not display noticeable fluorescence. Moreover, the fluorescence intensities of the dead cells reached a plateau after 1 min (for *E. coli*)/30 s (for *S. aureus*) (Figures 3D and 4D), demonstrating that the dead bacterial cell staining by S-OSiNDs is very fast. Besides, the results of the cellular fluorescence intensities obtained by flow cytometry (Figures 1B–D and 2B–D) agreed well with the confocal imaging results (Figures 3A and 4A).
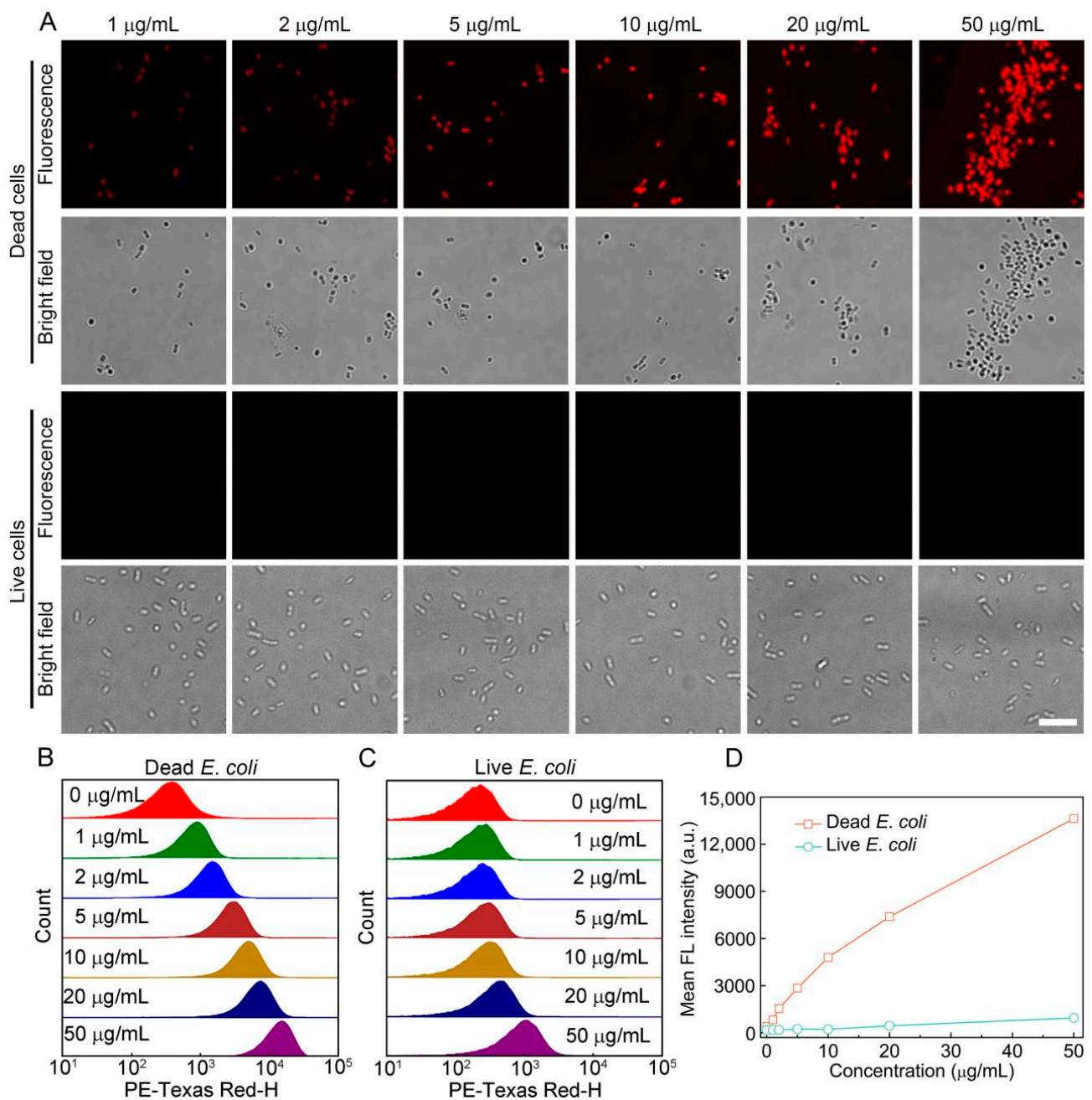

Figure 1. (**A**) Confocal images of dead and live *E. coli* cells incubated with various concentrations of S-OSiNDs for 30 s. Scale bar = 10 μm. Flow cytometric results of the dead (**B**) and live (**C**) *E. coli* cells incubated with different concentrations of S-OSiNDs for 30 s and (**D**) corresponding quantitative mean fluorescence intensities derived from the flow cytometric results.
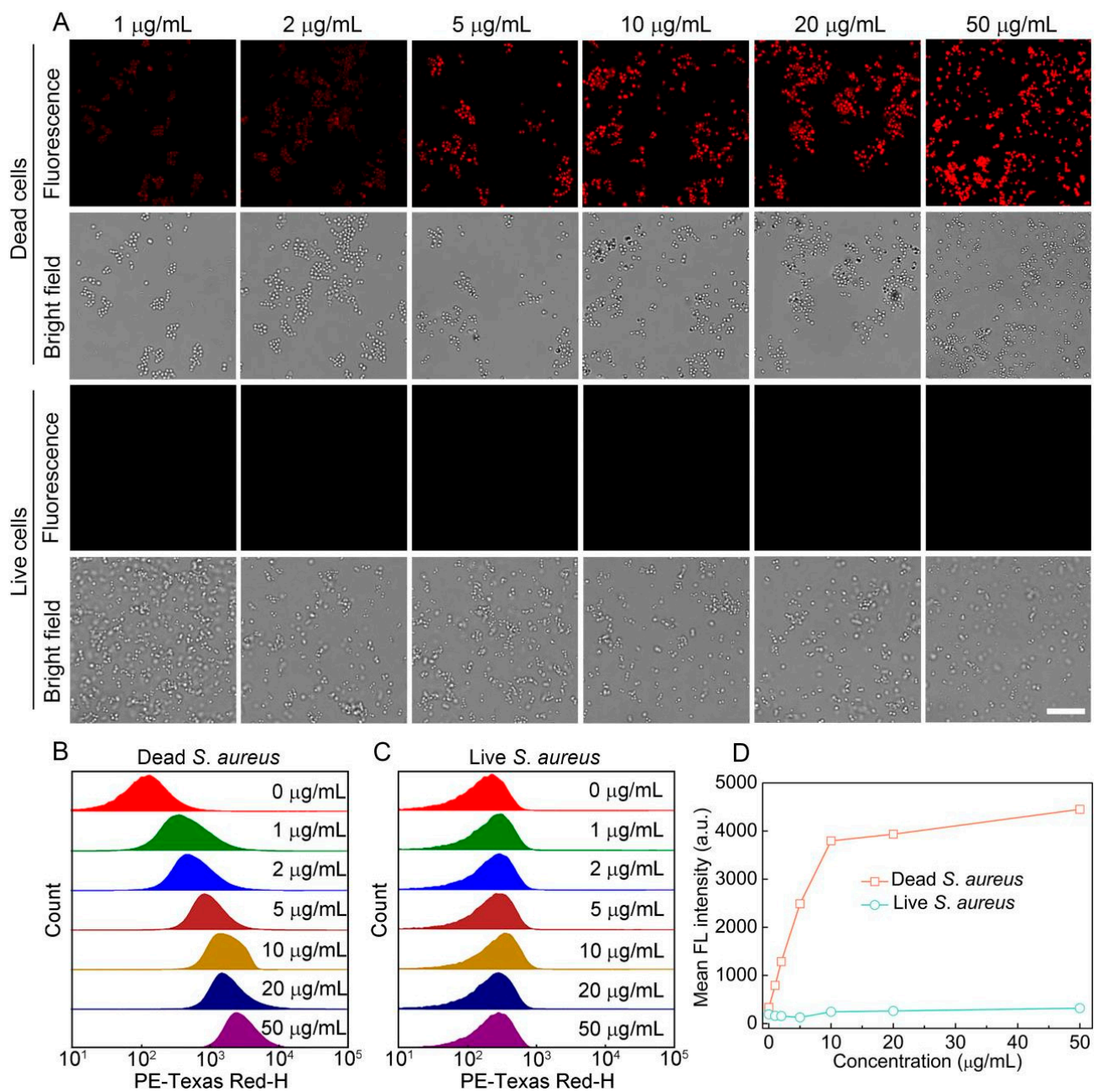
Figure 2. (**A**) Confocal images of dead and live *S. aureus* cells incubated with various concentrations of S-OSiNDs for 30 s. Scale bar = 10 μm. Flow cytometric results of the dead (**B**) and live (**C**) *S. aureus* cells incubated with different concentrations of S-OSiNDs for 30 s and (**D**) corresponding quantitative mean fluorescence intensities derived from the flow cytometric results.
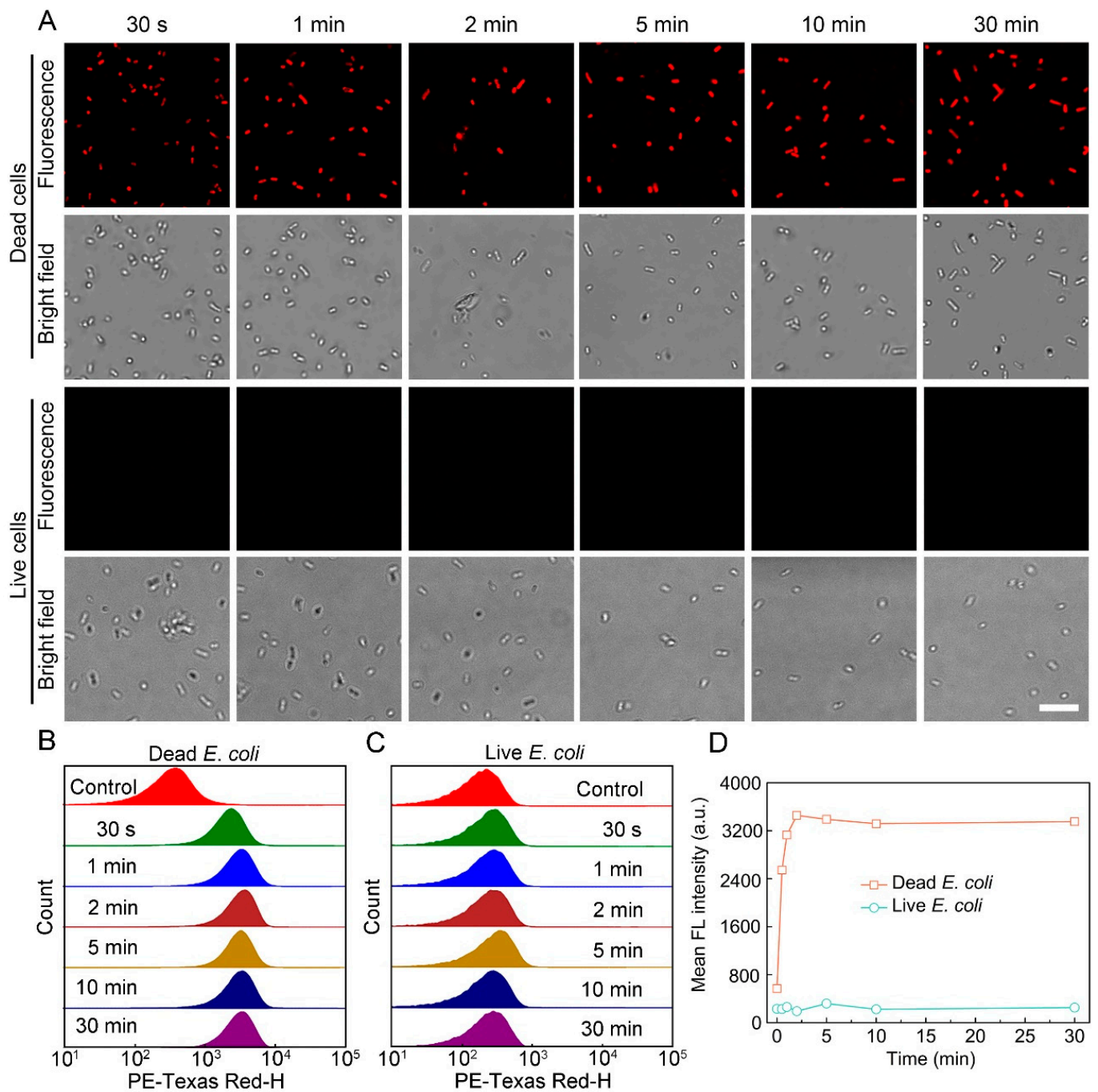
Figure 3. (**A**) Confocal images of dead and live *E. coli* cells treated with S-OSiNDs (5 μg/mL) for different time periods. Scale bar = 10 μm. Flow cytometric results of dead (**B**) and live (**C**) *E. coli* cells incubated without (control) or with S-OSiNDs (5 μg/mL) for different time periods and (**D**) corresponding quantitative mean fluorescence intensities derived from the flow cytometric results.
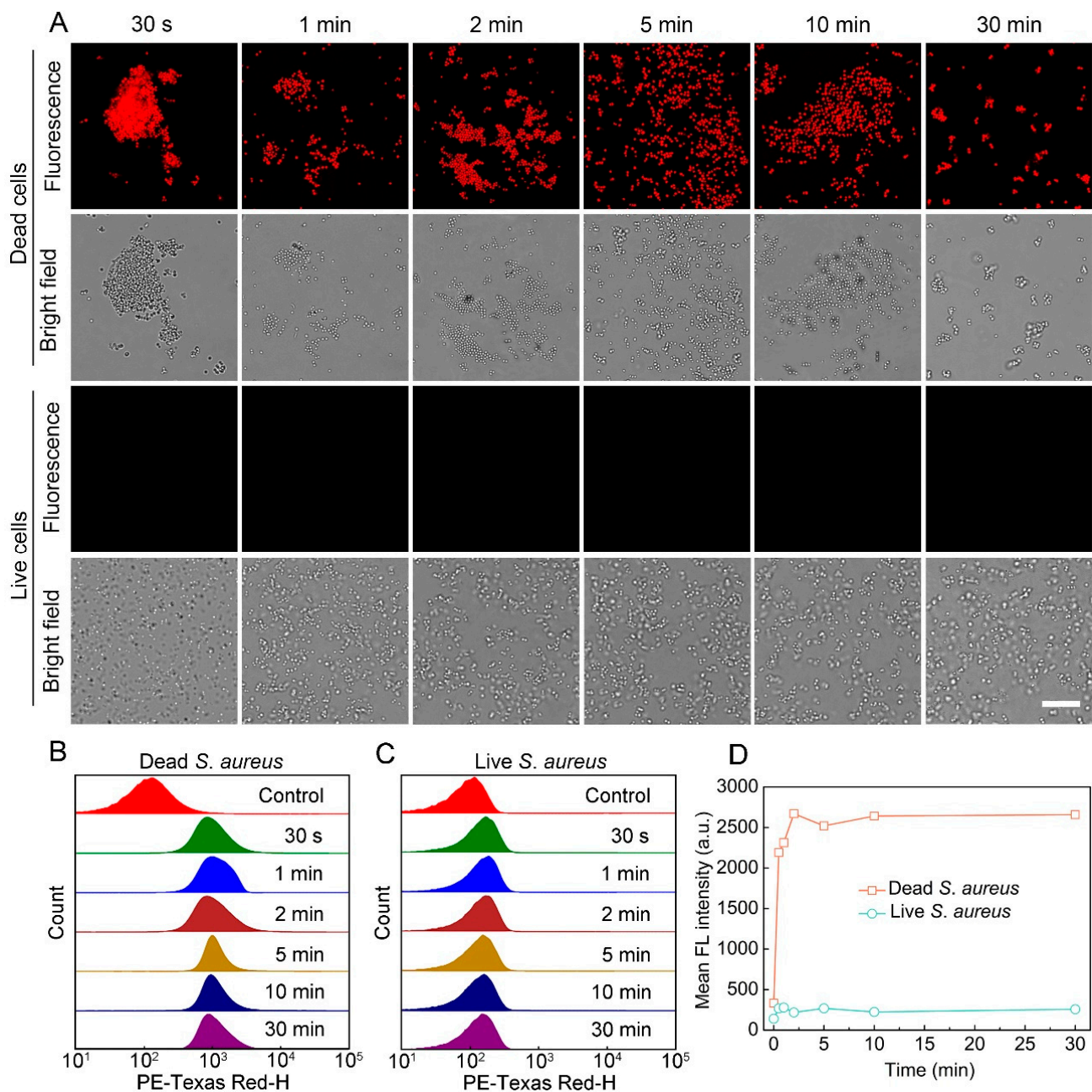
Figure 4. (**A**) Confocal images of dead and live *S. aureus* cells treated with S-OSiNDs (5 μg/mL) for different time periods. Scale bar = 10 μm. Flow cytometric results of the dead (**B**) and live (**C**) *S. aureus* cells incubated without (control) or with S-OSiNDs (5 μg/mL) for different time periods and (**D**) corresponding quantitative mean fluorescence intensities derived from the flow cytometric results.

Furthermore, we compared the fluorescence intensities between the S-OSiND-stained *E. coli* and *S. aureus*. According to the flow cytometric results (Figures 1D, 2D, 3D and 4D), the fluorescence intensities of the dead *E. coli* cells were higher than those of the dead *S. aureus* cells at the same S-OSiND concentrations/incubation time (at the plateau stages). This is because the size/volume of *E. coli* is larger than that of *S. aureus*, and therefore a higher intracellular content of S-OSiNDs can be found in the dead *E. coli* cells than that in the dead *S. aureus* cells.

Collectively, the above results demonstrated that S-OSiNDs were able to achieve rapid and accurate differentiation between live and dead bacterial cells.

3.2. Staining Performance of S-OSiNDs for Live and Dead Fungi

Besides the bacterial cells, we also tested the capacity S-OSiNDs to distinguish between live and dead fungal cells. To this end, the *S. cerevisiae* yeast was chosen. As shown in Figure 5A, only dead yeasts were successfully stained by the synthesized S-OSiNDs with strong red fluorescence, while the live yeasts did not show any fluorescence (compared with the untreated control group). In addition, the fluorescence intensities of the dead and live yeasts were measured using flow cytometry. The results showed that at all the tested concentrations, the cellular content of S-OSiNDs in the dead yeasts was much higher than that in the live cells (Figure 5B–D). Moreover, we further investigated the effect of incubation time on the live/dead cell discrimination performance of S-OSiNDs. It could be found that strong red fluorescence signals could be seen in the dead cells after incubation with S-OSiNDs for 30 s or longer, whereas the live cells that were treated with S-OSiNDs for different time periods did not display noticeable fluorescence (Figure 6A). In addition, as revealed by the corresponding flow cytometric results (Figure 6B–D), the fluorescence intensity of the dead yeasts reached a plateau after 30 s, demonstrating the rapid S-OSiND staining effect toward dead yeasts.
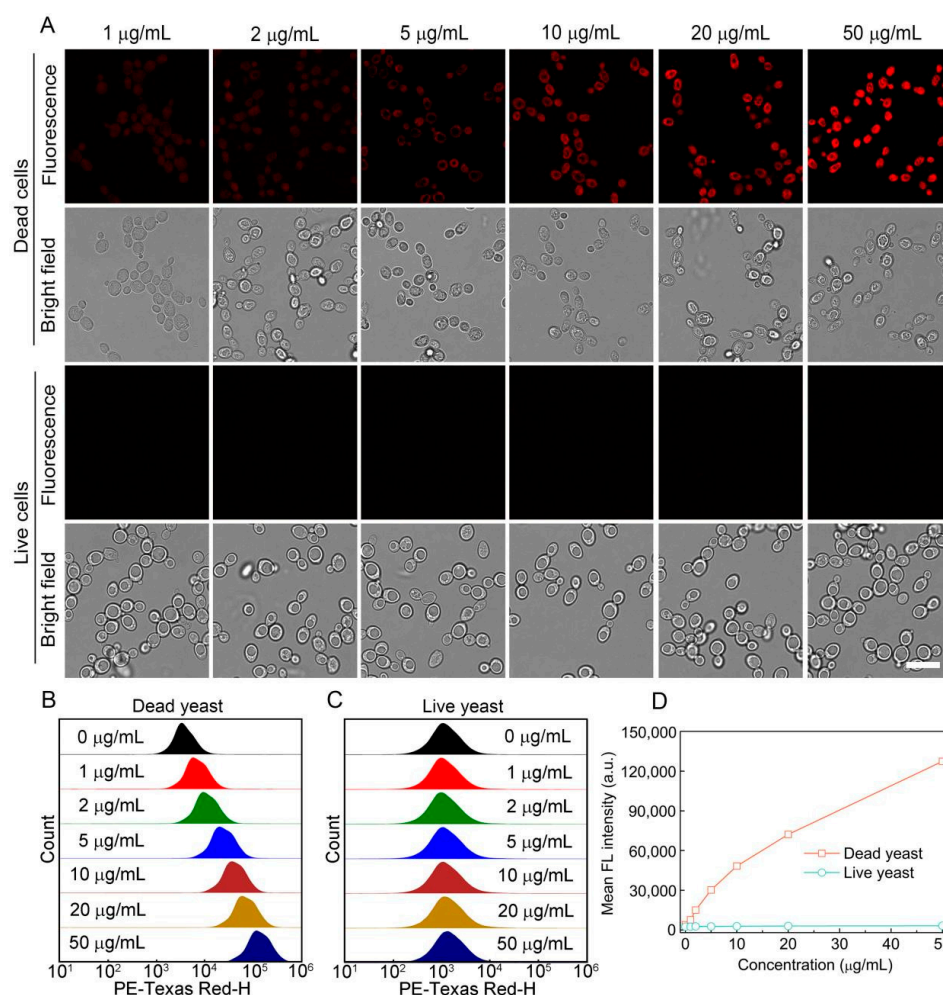

Figure 5. (**A**) Confocal images of dead and live *S. cerevisiae* cells incubated with various concentrations of S-OSiNDs for 30 s. Scale bar = 10 μm. Flow cytometric results of the dead (**B**) and live (**C**) *S. cerevisiae* cells incubated with different concentrations of S-OSiNDs for 30 s and (**D**) corresponding quantitative mean fluorescence intensities derived from the flow cytometric results.
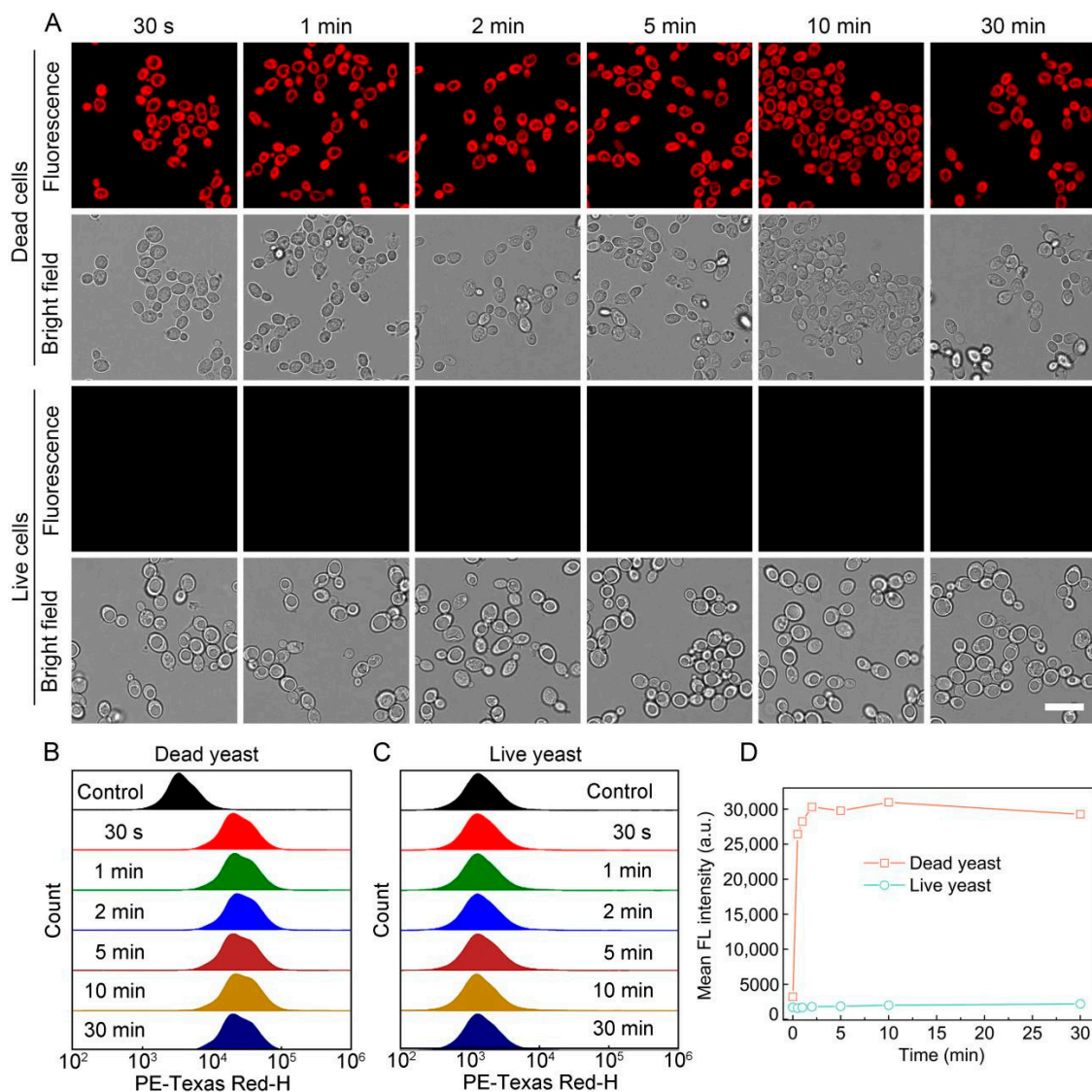
Figure 6. (**A**) Confocal images of dead and live *S. cerevisiae* cells treated with S-OSiNDs (5 μg/mL) for different time periods. Scale bar = 10 μm. Flow cytometric results of the dead (**B**) and live (**C**) *S. cerevisiae* cells incubated without (control) or with S-OSiNDs (5 μg/mL) for different time periods and (**D**) corresponding quantitative mean fluorescence intensities derived from the flow cytometric results.

To check the sensitivity of live/dead fungal cell discrimination of S-OSiNDs, we first defined the discrimination sensitivity as I_{dead}/I_{live} (in which I_{dead} represents the fluorescence intensity of dead cells, and I_{live} represents the fluorescence intensity of live cells). When the value of I_{dead}/I_{live} is above 1, the live and dead cells can be theoretically discriminated. In addition, the larger the value of I_{dead}/I_{live} is, the better the live/dead cell discrimination effect is. As shown in Figure 6D, after staining for 30 s, we could see that the value of I_{dead}/I_{live} was 15.3–16.8, which is much larger than 1, indicating that the discrimination is successful. In addition, Figure 5D exhibited that the fluorescence intensity of dead cells was concentration-dependent, and a higher S-OSiND concentration resulted in a stronger fluorescence emission, which accordingly led to a higher I_{dead}/I_{live} value and a higher discrimination sensitivity.

Collectively, the above results suggested that S-OSiNDs could achieve fast and accurate live/dead fungal cell discrimination.

3.3. Staining Performance of S-OSiNDs for Normal and Cancerous Mammalian Cells

Inspired by the above-mentioned live/dead microbial cell discrimination results of S-OSiNDs, we further tested the feasibility of using S-OSiNDs for distinguishing between live/dead normal/cancerous mammalian cells. We chose the normal HPAEpiCs and the cancerous A549 cells as two representative mammalian cell lines for the live/dead cell staining assay. As shown in Figures 7 and 8, the dead HPAEpiCs and A549 cells could be selectively labeled by different concentrations of S-OSiNDs, whereas almost no fluorescence was detected from the live cells even when the concentration increased to 50 μg/mL (Figures 7A and 8A). The corresponding flow cytometric results in Figures 7B–D and 8B–D further indicated that in all cases, the dead cells exhibited much higher fluorescence intensities than the live cells. The fluorescence intensity of the dead cells was concentration-dependent, and a dramatically enhanced fluorescence could be observed even at a very low S-OSiND concentration of 1 μg/mL.
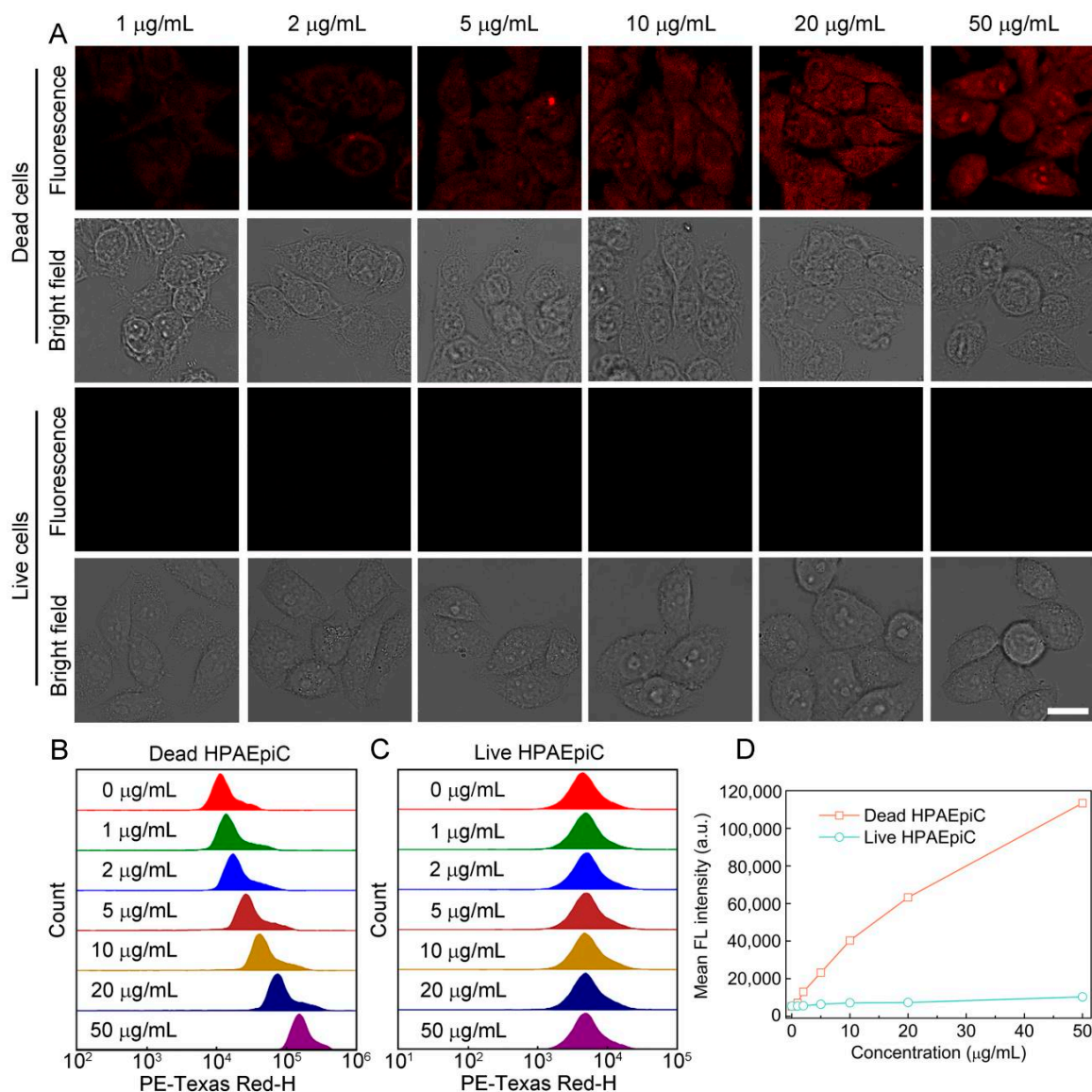

Figure 7. (**A**) Confocal images of dead and live HPAEpiCs incubated with various concentrations of S-OSiNDs for 30 s. Scale bar = 25 μm. Flow cytometric results of dead (**B**) and live (**C**) HPAEpiCs incubated with different concentrations of S-OSiNDs for 30 s and (**D**) corresponding quantitative mean fluorescence intensities derived from the flow cytometric results.

Figure 8. (**A**) Confocal images of dead and live A549 cells incubated with various concentrations of S-OSiNDs for 30 s. Scale bar = 25 μm. Flow cytometric results of dead (**B**) and live (**C**) A549 cells incubated with different concentrations of S-OSiNDs for 30 s and (**D**) corresponding quantitative mean fluorescence intensities derived from the flow cytometric results.
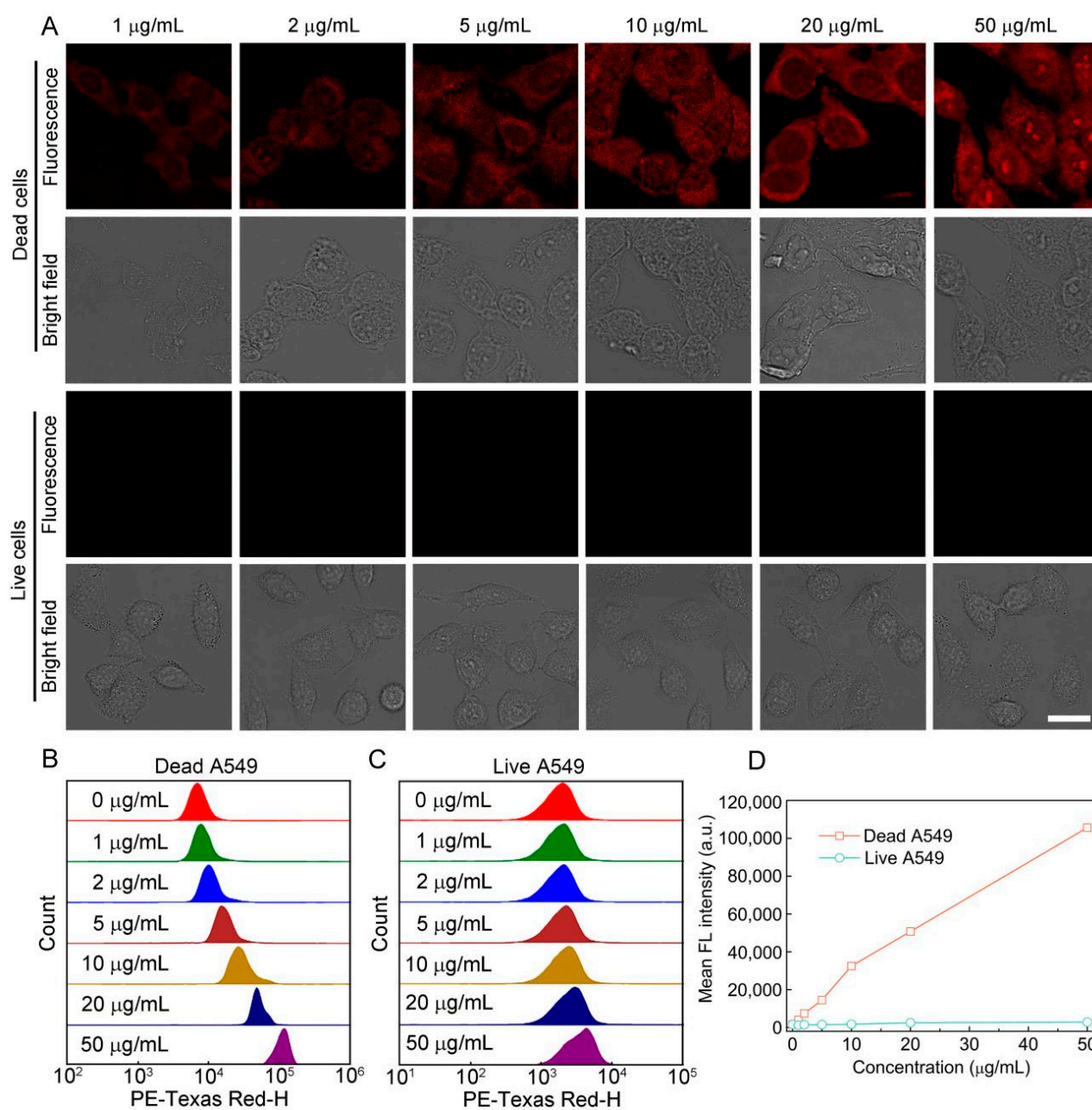
Moreover, we checked the effect of staining time on the live/dead mammalian cell differentiation performance of S-OSiNDs. As shown in Figures 9A and 10A, after incubation for only 30 s, the dead cells could be successfully stained by S-OSiNDs with strong red fluorescence, and the red fluorescence signals were distributed in the entire cells, including cytoplasm and nucleus, whereas no fluorescence was detected in the live cells even when the staining time was increased to 30 min. The results of the cellular fluorescence intensities obtained by flow cytometry (Figures 9B–D and 10B–D) were consistent with the confocal imaging results. Additionally, according to the flow cytometric results in Figures 9B–D and 10B–D, we could clearly see that there were no evident changes in the fluorescence intensity of the dead HPAEpiCs and A549 cells with the increase of staining time after 30 s.
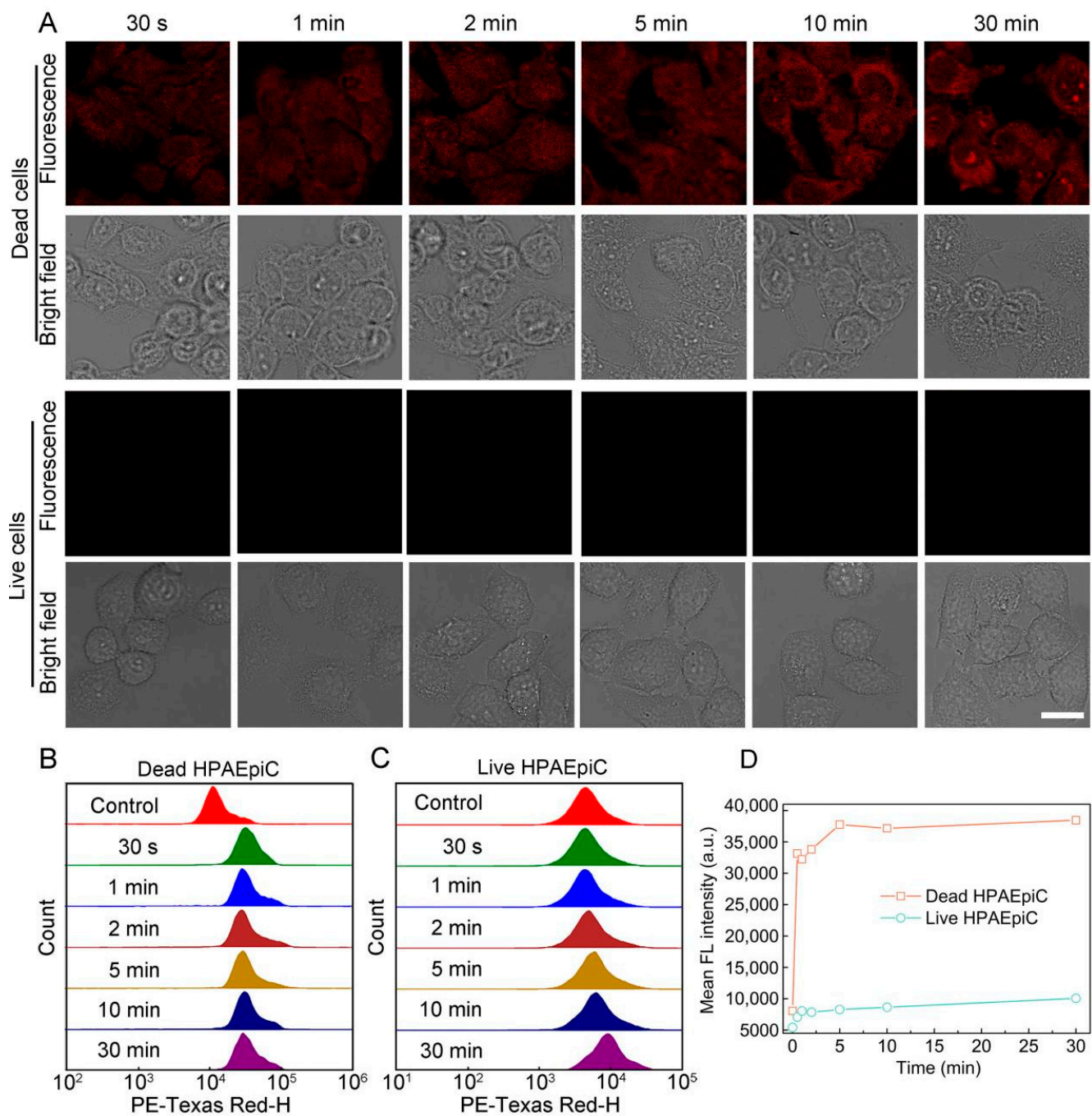
Figure 9. (**A**) Confocal images of dead and live HPAEpiCs treated with S-OSiNDs (5 µg/mL) for different time periods. Scale bar = 25 µm. Flow cytometric results of dead (**B**) and live (**C**) HPAEpiCs incubated without (control) or with S-OSiNDs (5 µg/mL) for different time periods and (**D**) corresponding quantitative mean fluorescence intensities derived from the flow cytometric results.

Figure 10. (**A**) Confocal images of dead and live A549 cells treated with S-OSiNDs (5 μg/mL) for different time periods. Scale bar = 25 μm. Flow cytometric results of dead (**B**) and live (**C**) A549 cells incubated without (control) or with S-OSiNDs (5 μg/mL) for different time periods and (**D**) corresponding quantitative mean fluorescence intensities derived from the flow cytometric results.
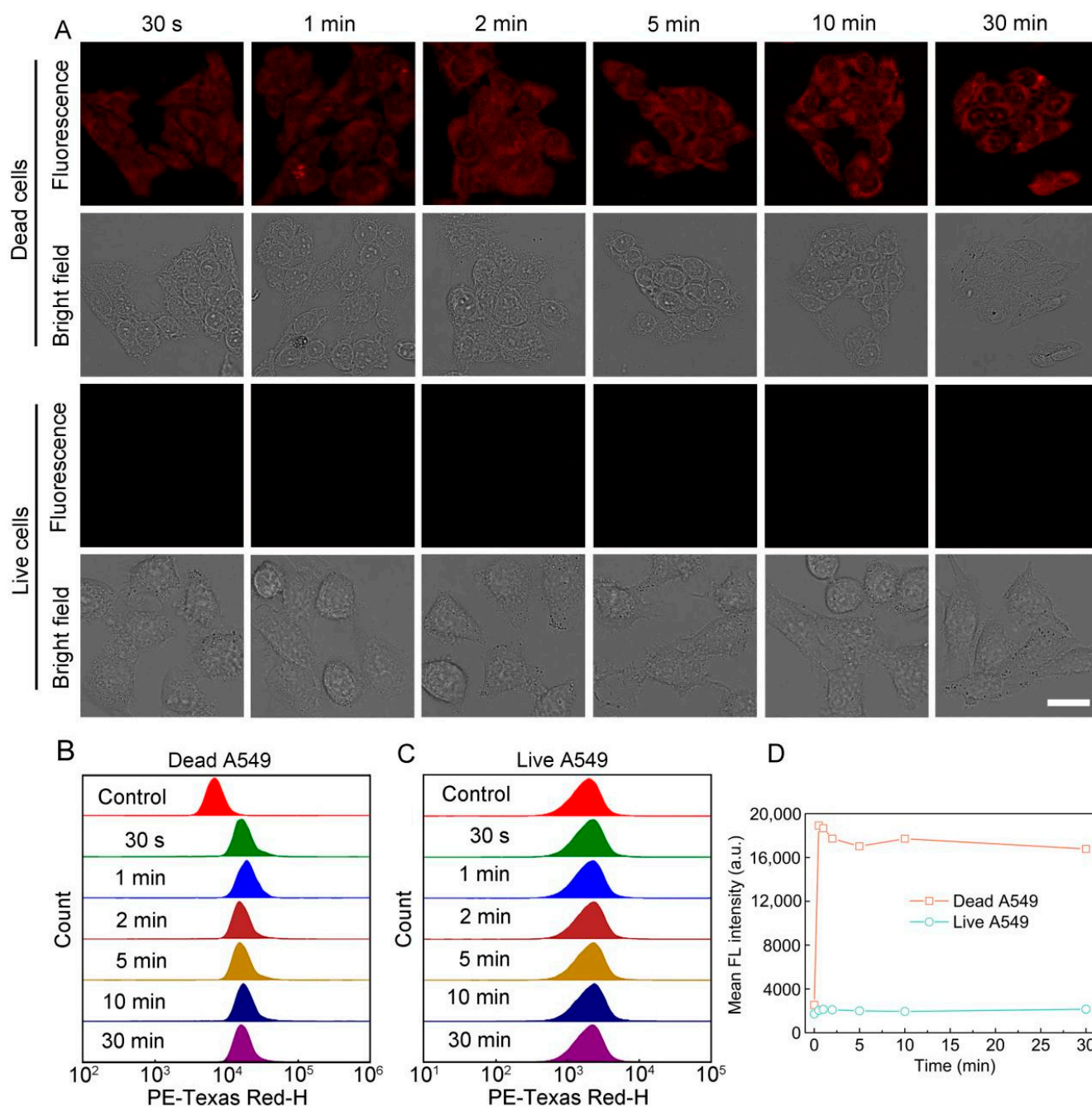
Furthermore, we compared the fluorescence intensities between the HPAEpiCs and A549 cells. It was found that the fluorescence intensities of the dead HPAEpiCs were higher than those of the dead A549 cells at the same S-OSiND concentrations/incubation time (at the plateau stages) (Figures 7D, 8D, 9D and 10D). Besides, according to the flow cytometric results (data not shown), the size/volume of HPAEpiCs is larger than that of A549 cells. Therefore, more intracellular S-OSiNDs can be accommodated in the dead HPAEpiCs than in the dead A549 cells.

Collectively, S-OSiNDs represent a promising and universal fluorescent probe for successfully discriminating between live and dead cells and realizing ultrafast (30 s) and sensitive staining (required dose of S-OSiNDs: 1 µg/mL) of dead cells.

3.4. Comparison between S-OSiNDs and RedDot2 on the Discrimination between Live and Dead Cells

To further evaluate the capability of S-OSiNDs in live/dead cell discrimination and uncover the selective labeling mechanism of dead cells, we treated the live and dead cells with the mixtures of S-OSiNDs and RedDot2. As shown in Figure 11, little fluorescence was observed in the live cells, revealing that the live cells were neither stained by S-OSiNDs nor RedDot2. On the other hand, strong yellow fluorescence could be observed in the merged confocal images of dead cells, confirming that S-OSiNDs (shown as green in the images) and RedDot2 (red fluorescence) can both selectively light up the dead cells and the dead cell staining mechanism of S-OSiNDs is the same as that of RedDot2. Specifically, for the dead HPAEpiCs and A549 cells, the red fluorescence of RedDot2 was mainly located in the nucleus, while the green signals (pseudo color) of S-OSiNDs were distributed in both the cytoplasm and nucleus, which illustrated that the fluorescence distribution range of S-OSiNDs was much larger than that of RedDot2 under the same staining condition. The larger fluorescence distribution range of S-OSiNDs indicated their better staining ability of the dead cells than that of RedDot2, which may help them to realize more sensitive and accurate discrimination of dead and live cells.
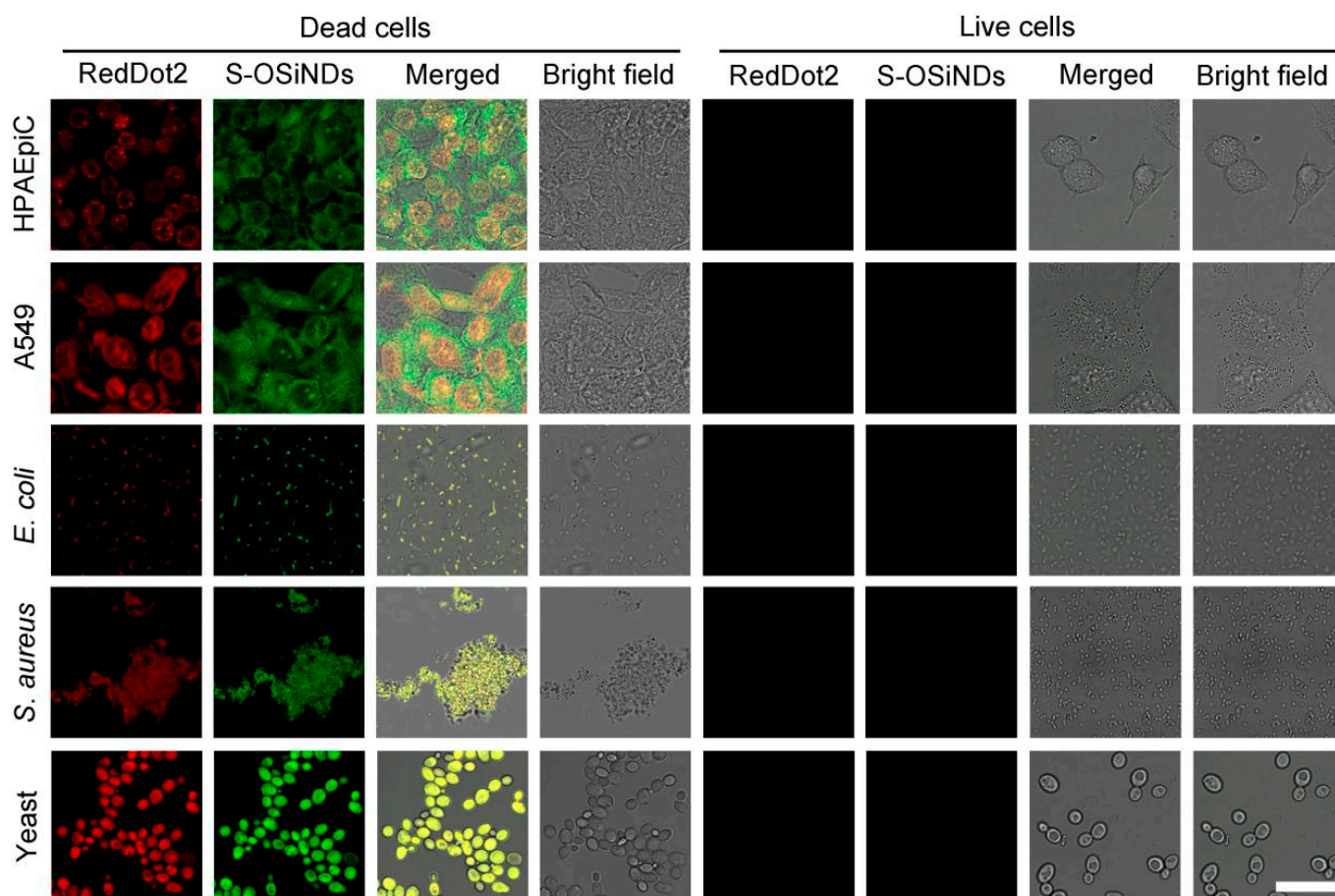

Figure 11. Confocal images of live/dead cells (HPAEpiC, A549, *E. coli*, *S. aureus*, and *S. cerevisiae* yeast) stained with S-OSiNDs (5 µg/mL) and RedDot2 (diluted with PBS (for mammalian cells)/physiological saline (for bacteria and fungi) using a 1:200 ratio) for 10 min. Note that the fluorescence emission color of S-OSiNDs was set as green.

3.5. Cytotoxicity Evaluation of S-OSiNDs

Next, the cytotoxicity of S-OSiNDs to the bacterial, fungal, and mammalian cells was also evaluated. The corresponding results are shown in Figure 12. It could be found that S-OSiNDs had negligible toxicity to *E. coli*, *S. aureus*, and yeast cells at concentrations of 50 μg/mL. Even when the concentration increased to 500 μg/mL, S-OSiNDs only had slight toxicity to *E. coli* (viability: ~76%), *S. aureus* (viability: ~84%), and yeast (viability: ~85%). When the concentration of S-OSiNDs was 500 μg/mL, the relative viabilities of HPAEpiCs and A549 cells were ~93% and ~99%, respectively. It is worth noting that the S-OSiND concentration of 500 μg/mL is much higher than the working concentration of 5 μg/mL. These results revealed the superb cytocompatibility of S-OSiNDs, ensuring their practical applications in cell imaging.
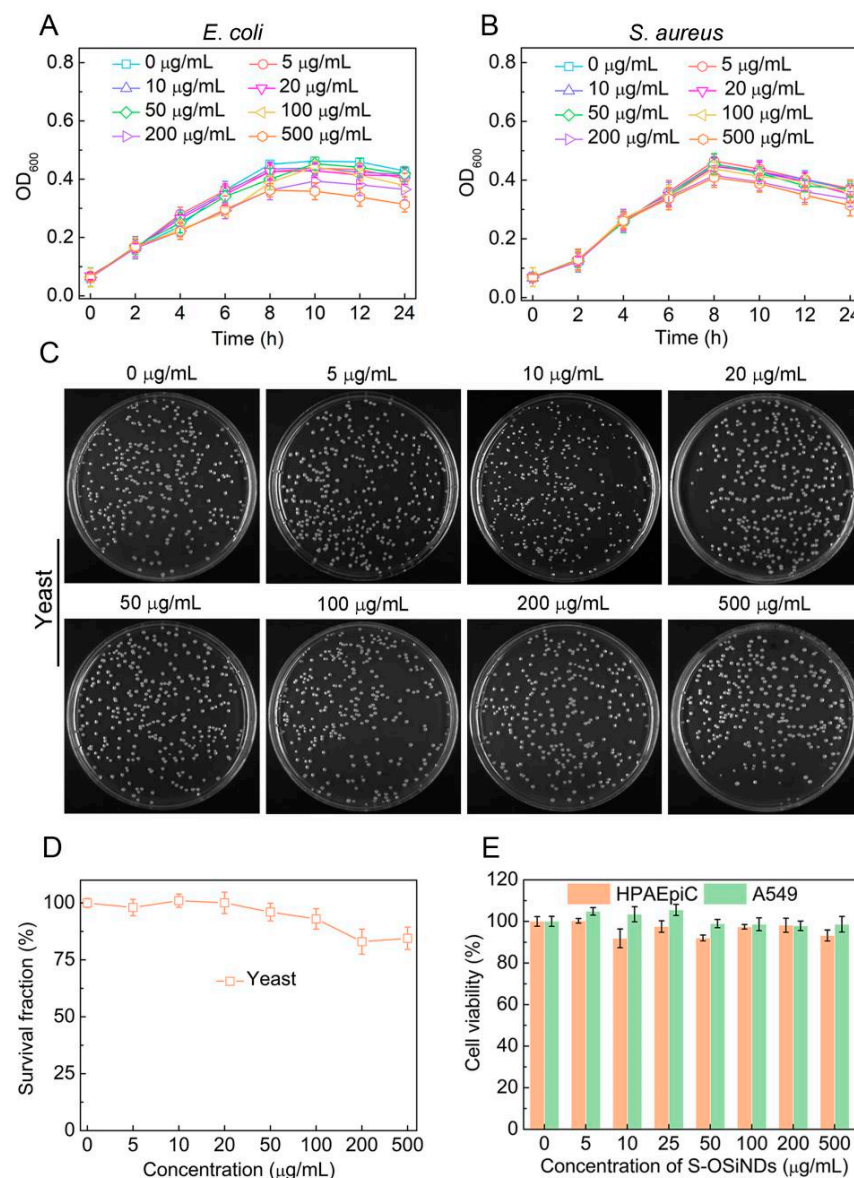

Figure 12. Cytotoxicity evaluation results of S-OSiNDs toward bacterial, fungal, and mammalian cells. Optical density at 600 nm (OD_{600}) values of (**A**) *E. coli* and (**B**) *S. aureus* bacterial suspensions treated with various concentrations of S-OSiNDs for different time periods. (**C**) Photographs of the agar plates showing the formed colonies of *S. cerevisiae* yeasts that were treated with various concentrations of S-OSiNDs for 24 h and (**D**) corresponding statistical data. (**E**) Relative viabilities of HPAEpiCs and A549 cells after treatment with different concentrations of S-OSiNDs for 24 h.

4. Conclusions

In this work, we demonstrated that S-OSiNDs could realize sensitive (1 μg/mL), ultra-fast (30 s), and selective fluorescence staining of dead bacterial, fungal, and mammalian cells. We have also proved that S-OSiNDs possessed good cytocompatibility. As a result, S-OSiNDs can be adopted as a robust fluorescent probe for successful fluorescence discrimination between live and dead cells regardless of the cell type. For mammalian cells, we confirmed that the fluorescence distribution range of S-OSiNDs (which are distributed in the cytoplasm and nucleus) is much larger than that of RedDot2 (which is distributed in the nucleus). These advantages demonstrate the bright application prospect of S-OSiNDs in cell imaging and cell viability evaluation. We surely believe that the S-OSiNDs can find a variety of applications in the biomedical field.

Supplementary Materials: The following supporting information can be downloaded at: https://www.mdpi.com/article/10.3390/bios12111000/s1, Figure S1: Characterizations of S-OSiNDs.

References

1. Kepp, O.; Galluzzi, L.; Lipinski, M.; Yuan, J.; Kroemer, G. Cell death assays for drug discovery. *Nat. Rev. Drug Discov.* **2011**, *10*, 221–237. [CrossRef] [PubMed]
2. Emerson, J.B.; Adams, R.I.; Román, C.M.B.; Brooks, B.; Coil, D.A.; Dahlhausen, K.; Ganz, H.H.; Hartmann, E.M.; Hsu, T.; Justice, N.B.; et al. Schrödinger's microbes: Tools for distinguishing the living from the dead in microbial ecosystems. *Microbiome* **2017**, *5*, 86. [CrossRef] [PubMed]
3. Chen, X.; Zhang, X.; Li, C.; Sayed, S.M.; Sun, W.; Lin, F.; Wu, F.G. Superbright orgnaosilica nanodots as a universal sensor for fast discrimination and accurate quantification of live/dead cells. *Sens. Actuat B-Chem.* **2019**, *295*, 49–55. [CrossRef]
4. Hu, X.; Wang, S.; Luo, Q.; Ge, B.; Cheng, Q.; Dong, C.; Xu, J.; Ding, H.; Xu, M.; Tedesco, A.C.; et al. Synthesis of Sn nanocluster@carbon dots for photodynamic therapy application. *Chin. Chem. Lett.* **2021**, *32*, 2287–2291. [CrossRef]
5. Zhou, L.; Qiu, T.; Lv, F.; Liu, L.; Ying, J.; Wang, S. Self-assembled nanomedicines for anticancer and antibacterial applications. *Adv. Healthc. Mater.* **2018**, *7*, 1800670. [CrossRef]
6. Liu, J.; Lu, S.; Tang, Q.; Zhang, K.; Yu, W.; Sun, H.; Yang, B. One-step hydrothermal synthesis of photoluminescent carbon nanodots with selective antibacterial activity against *Porphyromonas gingivalis*. *Nanoscale* **2017**, *9*, 7135–7142. [CrossRef]
7. Berghe, T.V.; Grootjans, S.; Goossens, V.; Dondelinger, Y.; Krysko, D.V.; Takahashi, N.; Vandenabeele, P. Determination of apoptotic and necrotic cell death in vitro and in vivo. *Methods* **2013**, *61*, 117–129. [CrossRef]
8. Fantner, G.E.; Barbero, R.J.; Gray, D.S.; Belcher, A.M. Kinetics of antimicrobial peptide activity measured on individual bacterial cells using high-speed atomic force microscopy. *Nat. Nanotechnol.* **2010**, *5*, 280–285. [CrossRef]
9. Davis, R.; Deering, A.; Burgula, Y.; Mauer, L.J.; Reuhs, B.L. Differentiation of live, dead and treated cells of *Escherichia coli* O157:H7 using FT-IR Spectroscopy. *J. Appl. Microbiol.* **2012**, *112*, 743–751. [CrossRef]
10. Krysko, D.V.; Vanden Berghe, T.; D' Herde, K.; Vandenabeele, P. Apoptosis and necrosis: Detection, discrimination and phagocytosis. *Methods* **2008**, *44*, 205–221. [CrossRef]
11. Tawakoli, P.N.; Al-Ahmad, A.; Hoth-Hannig, W.; Hannig, M.; Hannig, C. Comparison of different live/dead stainings for detection and quantification of adherent microorganisms in the initial oral biofilm. *Clin. Oral Inv.* **2013**, *17*, 841–850. [CrossRef] [PubMed]
12. Zhou, H.; Yang, D.; Ivleva, N.P.; Mircescu, N.E.; Schubert, S.; Niessner, R.; Wieser, A.; Haisch, C. Label-free in situ discrimination of live and dead bacteria by surface-enhanced Raman scattering. *Anal. Chem.* **2015**, *87*, 6553–6561. [CrossRef] [PubMed]
13. Li, R.; Dhankhar, D.; Chen, J.; Krishnamoorthi, A.; Cesario, T.C.; Rentzepis, P.M. Identification of live and dead bacteria: A Raman spectroscopic study. *IEEE Access* **2019**, *7*, 23549–23559. [CrossRef]

14. Baymiev, A.K.; Baymiev, A.K.; Kuluev, B.R.; Shvets, K.Y.; Yamidanov, R.S.; Matniyazov, R.T.; Chemeris, D.A.; Zubov, V.V.; Alekseev, Y.I.; Mavzyutov, A.R.; et al. Modern approaches to differentiation of live and dead bacteria using selective amplification of nucleic acids. *Microbiology* **2020**, *89*, 13–27. [CrossRef]

15. Cheng, H.B.; Li, Y.; Tang, B.Z.; Yoon, J. Assembly strategies of organic-based imaging agents for fluorescence and photoacoustic bioimaging applications. *Chem. Soc. Rev.* **2020**, *49*, 21–31. [CrossRef] [PubMed]

16. Xu, W.; Chen, J.; Sun, S.; Tang, Z.; Jiang, K.; Song, L.; Wang, Y.; Liu, C.; Lin, H. Fluorescent and photoacoustic bifunctional probe for the detection of ascorbic acid in biological fluids, living cells and in vivo. *Nanoscale* **2018**, *10*, 17834–17841. [CrossRef]

17. Lan, M.; Zhao, S.; Wu, S.; Wei, X.; Fu, Y.; Wu, J.; Wang, P.; Zhang, W. Optically tunable fluorescent carbon nanoparticles and their application in fluorometric sensing of copper ions. *Nano Res.* **2019**, *12*, 2576–2583. [CrossRef]

18. Park, S.H.; Kwon, N.; Lee, J.H.; Yoon, J.; Shin, I. Synthetic ratiometric fluorescent probes for detection of ions. *Chem. Soc. Rev.* **2020**, *49*, 143–179. [CrossRef]

19. Wang, H.Y.; Hua, X.W.; Jia, H.R.; Li, C.; Lin, F.; Chen, Z.; Wu, F.G. Universal cell surface imaging for mammalian, fungal, and bacterial cells. *ACS Biomater. Sci. Eng.* **2016**, *2*, 987–997. [CrossRef]

20. Tian, M.; Sun, J.; Tang, Y.; Dong, B.; Lin, W. Discriminating live and dead cells in dual-color mode with a two-photon fluorescent probe based on ESIPT mechanism. *Anal. Chem.* **2018**, *90*, 998–1005. [CrossRef]

21. Zhao, E.; Hong, Y.; Chen, S.; Leung, C.W.T.; Chan, C.Y.K.; Kwok, R.T.K.; Lam, J.W.Y.; Tang, B.Z. Highly fluorescent and photostable probe for long-term bacterial viability assay based on aggregation-induced emission. *Adv. Healthc. Mater.* **2014**, *3*, 88–96. [CrossRef] [PubMed]

22. Santoscoy, M.C.; Jarboe, L.R. Streamlined assessment of membrane permeability and its application to membrane engineering of *Escherichia coli* for octanoic acid tolerance tetraselmis suecica to evaluate vitality. *J. Ind. Microbiol. Biotechnol.* **2019**, *46*, 843–853. [CrossRef]

23. Roth, B.L.; Poot, M.; Yue, S.T.; Millard, P.J. Bacterial viability and antibiotic susceptibility testing with SYTOX green nucleic acid stain. *Appl. Environ. Microbiol.* **1997**, *63*, 2421–2431. [CrossRef]

24. Krämer, C.E.M.; Wiechert, W.; Kohlheyer, D. Time-resolved, single-cell analysis of induced and programmed cell death via non-invasive propidium iodide and counterstain perfusion. *Sci. Rep.* **2016**, *6*, 32104. [CrossRef] [PubMed]

25. Kaprelyants, A.S.; Kell, D.B. Rapid assessment of bacterial viability and vitality by rhodamine 123 and flow cytometry. *J. Appl. Bacteriol.* **1992**, *72*, 410–422. [CrossRef]

26. Jones, K.H.; Senft, J.A. An improved method to determine cell viability by simultaneous staining with fluorescein diacetate-propidium iodide. *J. Histochem. Cytochem.* **1985**, *33*, 77–79. [CrossRef] [PubMed]

27. MacIntyre, H.L.; Cullen, J.J. Classification of phytoplankton cells as live or dead using the vital stains fluorescein diacetate and 5-chloromethyl fluorescein diacetate. *J. Phycol.* **2016**, *52*, 572–589. [CrossRef]

28. Guilini, C.; Baehr, C.; Schaeffer, E.; Gizzi, P.; Rufi, F.; Haiech, J.; Weiss, E.; Bonnet, D.; Galzi, J.L. New fluorescein precursors for live bacteria detection. *Anal. Chem.* **2015**, *87*, 8858–8866. [CrossRef]

29. Grieshaber, P.; Lagrèze, W.A.; Noack, C.; Boehringer, D.; Biermann, J. Staining of fluorogold-prelabeled retinal ganglion cells with calcein-AM: A new method for assessing cell vitality. *J. Neurosci. Methods* **2010**, *192*, 233–239. [CrossRef]

30. Abdelkhaliq, A.; van der Zande, M.; Peters, R.J.B.; Bouwmeester, H. Combination of the BeWo b30 placental transport model and the embryonic stem cell test to assess the potential developmental toxicity of silver nanoparticles. *Part. Fibre Toxicol.* **2020**, *17*, 11. [CrossRef]

31. Song, Y.; Li, H.; Lu, F.; Wang, H.; Zhang, M.; Yang, J.; Huang, J.; Huang, H.; Liu, Y.; Kang, Z. Fluorescent carbon dots with highly negative charges as a sensitive probe for real-time monitoring of bacterial viability. *J. Mater. Chem. B* **2017**, *5*, 6008–6015. [CrossRef]

32. Lu, F.; Song, Y.; Huang, H.; Liu, Y.; Fu, Y.; Huang, J.; Li, H.; Qu, H.; Kang, Z. Fluorescent carbon dots with tunable negative charges for bio-imaging in bacterial viability assessment. *Carbon* **2017**, *120*, 95–102. [CrossRef]

33. Hua, X.H.; Bao, Y.W.; Wang, H.Y.; Chen, Z.; Wu, F.G. Bacteria-derived fluorescent carbon dots for microbial live/dead differentiation. *Nanoscale* **2017**, *9*, 2150–2161. [CrossRef] [PubMed]

34. Yu, X.W.; Liu, X.; Jiang, Y.W.; Li, Y.H.; Gao, G.; Zhu, Y.X.; Lin, F.; Wu, F.G. Rose bengal-derived ultrabright sulfur-doped carbon dots for fast discrimination between live and dead cells. *Anal. Chem.* **2022**, *94*, 4243–4251. [CrossRef] [PubMed]

35. Chen, J.; Liu, W.R.; Li, Y.; Zou, X.; Li, W.; Liang, J.; Zhang, H.; Liu, Y.; Zhang, X.; Hu, C.; et al. Architecting ultra-bright silanized carbon dots by alleviating the spin-orbit coupling effect: A specific fluorescent nanoprobe to label dead cells. *Chem. Eng. J.* **2022**, *428*, 131168. [CrossRef]

36. Yan, C.; Wang, C.; Hou, T.; Guan, P.; Qiao, Y.; Guo, L.; Teng, Y.; Hu, X.; Wu, H. Lasting tracking and rapid discrimination of live Gram-positive bacteria by peptidoglycan-targeting carbon quantum dots. *ACS Appl. Mater. Interfaces* **2021**, *13*, 1277–1287. [CrossRef]

37. Ji, X.; Wang, S.; Luo, Y.; Yuan, X.; Wei, Y.; Zhang, Q.; Qin, K.; Tu, Y. Green synthesis of *weissella*-derived fluorescence carbon dots for microbial staining, cell imaging and dual sensing of vitamin B$_{12}$ and hexavalent chromium. *Dyes Pigment.* **2021**, *184*, 108818. [CrossRef]

38. Yuan, X.; Tu, Y.; Chen, W.; Xu, Z.; Wei, Y.; Qin, K.; Zhang, Q.; Xiang, Y.; Zhang, H.; Ji, X. Facile synthesis of carbon dots derived from ampicillin sodium for live/dead microbe differentiation, bioimaging and high selectivity detection of 2, 4-dinitrophenol and Hg(II). *Dyes Pigment.* **2020**, *175*, 108187. [CrossRef]

39. Wang, Z.; Wu, F.G. Ultrasmall silicon nanoparticles for imaging and killing microorganisms: A minireview. *ChemNanoMat* **2022**, *8*, e202100369. [CrossRef]

40. Cui, M.; Li, D.; Du, X.; Li, N.; Rong, Q.; Li, N.; Shui, L.; Zhou, G.; Wang, X.; Brabec, C.J.; et al. A cost-effective, aqueous-solution-processed cathode interlayer based on organosilica nanodots for highly efficient and stable organic solar cells. *Adv. Mater.* **2020**, *32*, 2002973. [CrossRef]

41. Tang, J.; Chu, B.; Wang, J.; Song, B.; Su, Y.; Wang, H.; He, Y. Multifunctional nanoagents for ultrasensitive imaging and photoactive killing of Gram-negative and Gram-positive bacteria. *Nat. Commun.* **2019**, *10*, 4057. [CrossRef]

42. Chen, X.; Zhang, X.; Lin, F.; Guo, Y.; Wu, F.G. One-step synthesis of epoxy group-terminated organosilica nanodots: A versatile nanoplatform for imaging and eliminating multidrug-resistant bacteria and their biofilms. *Small* **2019**, *15*, 1901647. [CrossRef] [PubMed]

43. Guo, D.; Ji, X.; Peng, F.; Zhong, Y.; Chu, B.; Su, Y.; He, Y. Photostable and biocompatible fluorescent silicon nanoparticles for imaging-guided co-delivery of siRNA and doxorubicin to drug-resistant cancer cells. *Nano-Micro Lett.* **2019**, *11*, 27. [CrossRef] [PubMed]

44. Chen, X.; Zhang, X.; Guo, Y.; Zhu, Y.X.; Liu, X.; Chen, Z.; Wu, F.G. Smart supramolecular "Trojan horse"-inspired nanogels for realizing light-triggered nuclear drug influx in drug-resistant cancer cells. *Adv. Funct. Mater.* **2019**, *29*, 1807772. [CrossRef]

45. Cui, M.; Liu, S.; Song, B.; Guo, D.; Wang, J.; Hu, G.; Su, Y.; He, Y. Fluorescent silicon nanorods-based nanotheranostic agents for multimodal imaging-guided photothermal therapy. *Nano-Micro Lett.* **2019**, *11*, 73. [CrossRef]

46. Jiang, D.; Pan, Y.; Yao, H.; Sun, J.; Xiong, W.; Li, L.; Zheng, F.; Sun, S.; Zhu, J.J. Synthesis of renal-clearable multicolor fluorescent silicon nanodots for tumor imaging and in vivo H_2O_2 profiling. *Anal. Chem.* **2022**, *94*, 9074–9080. [CrossRef]

47. Huang, S.; Yu, L.; Su, P.; Wen, T.; Sun, M.; Huang, D.; Wang, X.; Wang, S. Surface enhanced FRET for sensitive and selective detection of doxycycline using organosilicon nanodots as donors. *Anal. Chim. Acta* **2022**, *1197*, 339530. [CrossRef]

48. Chu, B.; Song, B.; Ji, X.; Su, Y.; Wang, H.; He, Y. Fluorescent silicon nanorods-based ratiometric sensors for long-term and real-time measurements of intracellular pH in live cells. *Anal. Chem.* **2017**, *89*, 12152–12159. [CrossRef]

49. Wu, F.G.; Zhang, X.; Kai, S.; Zhang, M.; Wang, H.Y.; Myers, J.N.; Weng, Y.; Liu, P.; Gu, N.; Chen, Z. One-step synthesis of superbright water-soluble silicon nanoparticles with photoluminescence quantum yield exceeding 80%. *Adv. Mater. Interfaces* **2015**, *2*, 1500360. [CrossRef]

50. Zhang, X.; Chen, X.; Kai, S.; Wang, H.Y.; Yang, J.; Wu, F.G.; Chen, Z. Highly sensitive and selective detection of dopamine using one-pot synthesized highly photoluminescent silicon nanoparticles. *Anal. Chem.* **2015**, *87*, 3360–3365. [CrossRef]

51. Zeng, J.; Hua, X.W.; Bao, Y.W.; Wu, F.G. Orange-emissive sulfur-doped organosilica nanodots for metal ion/glutathione detection and normal/cancer cell identification. *ACS Appl. Nano Mater.* **2021**, *4*, 6083–6092. [CrossRef]

52. Zhong, Y.; Peng, F.; Bao, F.; Wang, S.; Ji, X.; Yang, L.; Su, Y.; Lee, S.T.; He, Y. Large-scale aqueous synthesis of fluorescent and biocompatible silicon nanoparticles and their use as highly photostable biological probes. *J. Am. Chem. Soc.* **2013**, *135*, 8350–8356. [CrossRef] [PubMed]

53. Zhong, Y.; Sun, X.; Wang, S.; Peng, F.; Bao, F.; Su, Y.; Li, Y.; Lee, S.T.; He, Y. Facile, large-quantity synthesis of stable, tunable-color silicon nanoparticles and their application for long-term cellular imaging. *ACS Nano* **2015**, *9*, 5958–5967. [CrossRef] [PubMed]

54. Chen, X.; Zhang, X.; Xia, L.Y.; Wang, H.Y.; Chen, Z.; Wu, F.G. One-Step synthesis of ultrasmall and ultrabright organosilica nanodots with 100% photoluminescence quantum yield: Long-term lysosome imaging in living, fixed, and permeabilized cells. *Nano Lett.* **2018**, *18*, 1159–1167. [CrossRef] [PubMed]